Article

Normative Data of Ocular Biometry, Optical Coherence Tomography, and Electrophysiology Conducted for Cynomolgus Macaque Monkeys

Kwang-Eon Choi[1], Vu Thi Que Anh[2], Cheolmin Yun[1], Young-Jin Kim[3], Hachul Jung[3], Heejong Eom[4], Dongkwan Shin[4], and Seong-Woo Kim[1]

[1] Department of Ophthalmology, Korea University College of Medicine, Seoul, Korea
[2] Department of Ophthalmology, Hanoi Medical University, Hanoi, Vietnam
[3] Medical Device Development Center, Osong Medical Innovation Foundation, Cheongju, Chungbuk, Korea
[4] Laboratory Animal Center, Osong Medical Innovation Foundation, Cheongju, Chungbuk, Korea

Correspondence: Seong-Woo Kim, Department of Ophthalmology, Korea University Guro Hospital 148, Gurodong-ro, Guro-gu, Seoul 08308, South Korea.
e-mail: ksw64723@korea.ac.kr

Purpose: To present normative data of optical coherence tomography (OCT) parameters, electrophysiological tests, and optical biometry conducted for cynomolgus monkeys.

Methods: Multimodal examinations were performed for 11 adult cynomolgus monkeys (*Macaca fascicularis*, weighing 2.6–7.5 kg, aged 45–99 months). A-scan biometry was performed to measure ocular biometry. OCT images were obtained at 30° and 55°. After the pupils were fully dilated, electroretinogram (ERG) and visual evoked potentials (VEP) were recorded with a commercial system using a contact lens electrode.

Results: All cynomolgus monkeys were males. The mean axial length was 17.92 ± 0.34 mm. The central total retinal layer (TRL) and subfoveal choroidal thicknesses were 286.27 ± 18.43 and 234.73 ± 53.93 μm, respectively. The TRL and nerve fiber layer thickness was greater in the nasal than in other quadrants in the Early Treatment Diabetic Retinopathy Study circle in the macula. Peripheral TRL and ganglion cell complex thickness on the temporal outside the vascular arcades were lower than on the other sides. The peak latency of a-wave and b-wave in scotopic and photopic 3.0 ERG was 14.78 ± 1.00 and 32.89 ± 1.81 ms, and 12.91 ± 1.03 and 31.79 ± 2.16 ms, respectively. The n2 wave peak latency of VEP was 15.21 ± 8.07 ms. The a-wave peak latency of ERG and the n2 wave peak latency of VEP negatively correlated with age.

Conclusions: The normative ocular biometric, electrophysiological test, and OCT parametric data of cynomolgus monkeys could serve as reference values for further preclinical studies.

Translational Relevance: We present normative data of cynomolgus monkeys' eyes, an adequate animal model for preclinical studies.

Introduction

Visual science studies, especially on retinal degeneration, have usually been actively performed using small animals such as rats and mice.[1,2] However, sometimes their eyes are too small for surgical manipulation; at times, the macula does not exist, and the cone cell number is too low.[3,4] Instead, several ophthalmic studies have used medium- to large-sized animals with larger eyeball sizes, such as rabbits and pigs,[5,6] which have visual streaks with dense photoreceptors and ganglion cells.[7,8] However, visual streaks are not consistent with the human macula. Conversely, nonhuman primates have the uniqueness of a similar model of human vision with the fovea.[9] Humans and monkeys share susceptibility genes for age-related macular degeneration and have genotype–phenotype correlations for some inherited retinal diseases such as retinitis pigmentosa.[9,10] Furthermore, as

nonhuman primate models are useful for understanding vision,[11,12] these models are used in studies related to translation therapies targeting the fovea and other interventions for complex eye diseases.[13] Among these, cynomolgus macaque (*Macaca fascicularis*) and rhesus macaque (*Macaca mulatta*) are typical nonhuman primates commonly used in biological research.[14]

Optical coherence tomography (OCT) is a noninvasive approach to evaluate the retina and choroid structures.[15] A previous study reported a correlation between anatomical histology and OCT findings.[16]

An electroretinogram (ERG) has been used to evaluate visual function in animal ophthalmic research. Many previous studies have evaluated ophthalmic functions using nonhuman primates.[17,18] Furthermore, one study correlating anatomy and visual function in rhesus macaques has been published.[19] However, most individual studies have reported anatomical structures, visual functions, and eye sizes, respectively. Therefore, it was difficult to present normative data simultaneously and evaluate the relationships between each factor directly because each nonhuman primate study with the same species had different weights, ages, and eyeball sizes in each study. To the best of our knowledge, there is a lack of studies reporting detailed sublayer thickness on the fovea with a simultaneous visual function examination in cynomolgus monkeys.

Therefore, we examined the sublayer thickness of the macula and peripheral retina in cynomolgus monkeys and simultaneously evaluated ERG and ocular biometry.

Methods

All monkeys in this study were cynomolgus macaques (*Macaca fascicularis*), supplied by the Korea National Primate Research Center, Jeongeup-si, Korea. Multimodal examinations, including spectral-domain OCT images, full-field ERG, and ocular biometry, were performed at the Osong Medical Innovation Foundation laboratory animal center. All tests were performed under general anesthesia with atropine (0.04 mg/kg), ketamine (15 mg/kg), and domitor (60 μg/kg) administered intramuscularly. Subsequently, maintenance was performed using 1.5% to 2.5% sevoflurane at 1 L/min with 100% oxygen supply. The eyes were fully dilated for the initial examination using three drops of a tropherine solution (phenylephrine hydrochloride 5 mg/mL + tropicamide 5 mg/mL). Eye drops were administered at 30-minute intervals to maintain the dilation well. All procedures were performed in accordance with the Association for Research in Vision and Ophthalmology's Statement for the Use of Animals in Ophthalmic and Vision Research. The study was approved by the Institutional Animal Care and Use Committee of the Osong Medical Innovation Foundation in Korea (KBIO-IACUC-2020-054).

Ocular Biometry

For ocular biometry, a lid speculum was inserted into each eye. A-scan biometry (SW-1000, Suoer, Shanghai, China) was used to measure the axial length (AL), anterior chamber depth (ACD), lens thickness (LT), and vitreous chamber thickness (VCD) in both monkey eyes.

Image Acquisition and Analysis

Infrared and OCT images in the 30° and 55° ranges were obtained using a Spectralis OCT (Heidelberg Engineering GmbH, Heidelberg, Germany) instrument. Vertical and horizontal line scans for a 55° image were obtained using the raster scan protocol (33 B-scans for a 16.5 × 16.5 mm area) in a high-resolution mode (1536 A-scans per B scan, lateral resolution: 10 μm/pixel). Similarly, scans for a 30° image (64 B-scans for a 4.5 × 4.5 mm area) were performed in the same mode (1536 A-scans per B scan, lateral resolution: 5 μm/pixel). The thicknesses of the total retinal layer (TRL), total choroidal layer, retinal nerve fiber layer, ganglion cell complex (GCC), ganglion cell layer (GCL), inner plexiform layer (IPL), inner nuclear layer (INL), outer plexiform layer (OPL), outer nuclear layer (ONL), inner retinal layer (IRL), and outer retinal layer (ORL) were evaluated for the macula and periphery. TRL was defined as the layer from the inner border of the internal limiting membrane to the outer border of the retinal pigment epithelium (RPE) layer. The IRL was considered as the layer from the inner border of the internal limiting membrane to the ellipsoid zone, and the layer from the ellipsoid zone to the outer border of the RPE layer was termed ORL and GCC was defined as the layer between the inner borders of the NFL and INL. The individual thickness values on the fovea, parafovea (1- to 3-mm zone), and perifovea (3- to 6-mm zone) were measured automatically in the Early Treatment Diabetic Retinopathy study circular to the macula using the in-built program. The measurements for 30° OCT were performed twice to ensure repeatability of the test, and the mean values were used for analysis. Peripheral thickness was measured at four points from the macula. With respect to the macula, measurements at the superior, inferior, temporal, and nasal points (at 5 mm each) were performed using a widefield

Table 1. ERG of Cynomolgus Monkeys

Standard Response (ISCEV)	a-Wave Amplitudes (μV)	a-Wave Peak Latency (ms)	b-Wave Amplitudes (μV)	b-Wave Peak Latency (ms)	Luminance (cd.s.m.$^{-2}$)	Inner Stimulus Time (Hz)	Adaptation State
Rod response			96.36 ± 24.46	71.99 ± 5.23	0.01	0.49	Dark
Maximal response	128.36 ± 31.68	14.78 ± 1.00	132.71 ± 26.34	32.89 ± 1.81	3.0	0.1	Dark
Oscillatory potential			32.34 ± 11.62		3.0	0.1	Dark
Strong flash response	90.97 ± 25.09	13.98 ± 0.94	79.70 ± 19.08	31.16 ± 1.51	10	0.05	Dark
White flash cone response	27.13 ± 7.39	12.91 ± 1.03	79.86 ± 19.21	31.79 ± 2.16	3.0	2.0	Light
30 Hz flicker			99.63 ± 26.21		3.0	30	Light

Values are mean ± standard deviation.
ISCEV, International Society for Clinical Electrophysiology of Vision.

55° lens (Supplementary Fig. S1). The thickness values were comparable when switching between the standard 30° spectral domain OCT and wide-field 55° spectral domain OCT.[20] For accuracy and the thicknesses of TRL, IRL, ORL, and GCC were measured at the periphery. Two researchers performed the measurements directly (K.E.C. and V.T.Q.A.), and the mean value was used for analysis.

Electrophysiology Test

The protocol for ERG was based on the standard of the International Society for Clinical Electrophysiology of Vision.[21] The luminance and inner stimulus time for scotopic 0.01 (rod response), 3.0 (maximal responses), oscillatory potentials, 10.0 (strong flash), photopic 3.0 (white flash cone response), and 30 Hz flicker ERG are summarized in Table 1. A background luminance of 30 cd m^{-2} was done for light adaptation, and a recording bandpass of 0.3 to 300.0 Hz was used. Each recording averaged at least 16 responses over a 2-second interstimulus interval. The pupils were enlarged to a diameter of 5 mm under general anesthesia and underwent dark adaptation for 30 minutes. Topical eye drops were administered to maintain pupil dilatation at 30-minute intervals until the end of the experiment. A commercial ERG system (RETIcom; Ronald Consult, Germany) with LED light stimulation recorded the ERG signal. Furthermore, a contact lens electrode with a built-in LED light source (Kooijman/Damhof ERG lens, Medical Workshop BV, the Netherlands) was used for light stimulation to enable consistent illumination.

The flash visual evoked potential (VEP) protocols were based on the ISCEV standard,[22] with a stimulus luminance of 3.0 cd·s·m^{-2} and a recording bandpass of 1 to 500 Hz. VEP stimulation was performed with the same RETIcom machine using a contact lens with a built-in light source. VEP activity was detected via platinum subdermal electrodes placed approximately 1 cm superior to the occipital ridge. Reference recording was placed approximately 3 cm posterior to the frontal suture targeted for the frontal lobe. The ground recording was placed in the upper arm.

Statistical Analysis

The Wilcoxon signed-rank test repeated analysis of variance with Bonferroni correction, Pearson's χ^2 test, Spearman's correlation coefficient, and multiple logistic regression tests were performed using SPSS (version 21.0; SPSS Inc., Chicago, IL). Statistical significance was set at a *P* value of less than 0.05.

Results

Animals

Eleven cynomolgus monkeys (22 eyes) were included in the study. All monkeys were male, and the mean age was 63.79 ± 20.36 months (range, 49–95 months; median, 52 months). The mean body weight was 4.29 ± 1.41 kg (range, 3.2–7.5 kg) (Table 2).

Ocular Biometry

The mean AL, ACD, LT, and VCD were 18.41 ± 0.52, 3.12 ± 0.38, 3.51 ± 0.52, and 11.77 ± 0.76 mm, respectively. AL was significantly correlated with VCD (r = 0.796, *P* < 0.001, Pearson's correlation coefficient) and ACD (r = 0.460, *P* = 0.031). The LT was negatively correlated with the ACD (r = 0.504, *P* = 0.017) and VCD (r = −0.627, *P* = 0.002). The ACD seemed to have significant correlations with the AL, LT, and GCC on the fovea, and the INL on the fovea. However, after

Table 2. Ocular Biometry for Cynomolgus Monkeys

	Both	Right eye	Left eye	P Value Between the Right Eye and Left Eye
Age (months)	63.79 ± 20.36			
Weight (kg)	4.29 ± 1.41			
AL (mm)	18.41 ± 0.52	18.43 ± 0.57	18.38 ± 0.48	0.505[*]
ACD (mm)	3.09 ± 0.32	3.13 ± 0.38	3.05 ± 0.27	0.185[*]
Lens (mm)	3.51 ± 0.52	3.49 ± 0.56	3.53 ± 0.51	0.9999[*]
VCD (mm)	11.77 ± 0.76	11.85 ± 0.79	11.69 ± 0.76	0.247[*]

Values are mean ± standard deviation.
ACD, anterior chamber depth; VCD, vitreous chamber depth.
[*]$P < 0.05$, based on Wilcoxon signed-rank test.

Table 3. Correlations Between OCT and Ocular Biometry

	R^2	Related Factors	First	Second
ACD	0.500	1. AL	B = 0.206	B = 0.019
		2. GCC (center)	$P = 0.049$[*]	$P = 0.001$[*]
VCD	0.809	1. AL	B = 0.939	B = −0.658
		2. LT	$P < 0.001$[*]	$P = 0.001$[*]
LT	0.460	1. VCD	B = −0.463	
			$P = 0.001$[*]	

VCD, vitreous chamber depth.
AL, axial length; ACD, anterior chamber depth; LT, lens thickness; VCD, vitreous chamber depth; GCC, ganglion cell complex.
[*]Multiple regression analysis.

multiple regression analysis, the ACD showed significant correlations ($R^2 = 0.500$) with the AL (B = 0.206, $P = 0.049$) and the GCC on the fovea (B = 0.019, $P = 0.001$). Although the VCD was significantly correlated ($R^2 = 0.809$) with the AL (B = 0.939, $P < 0.001$) and the VCD (B = −0.658, $P = 0.001$), the LT was negatively correlated ($R^2 = 0.460$) with the VCD (B = −0.463, $P = 0.001$) (Table 3 and Supplementary Fig. S2).

OCT Measurements

The mean TRL thickness of the fovea was 286.27 ± 18.43 μm, and the mean subfoveal choroidal layer thickness was 234.73 ± 53.93 μm. The fovea's mean IRL thickness and the mean ORL thickness were 176.91 ± 14.28 and 106.36 ± 26.07 μm, respectively. The mean GCC layer and the mean NFL thickness of the fovea were 56.73 ± 10.55 and 12.59 ± 1.44 μm, respectively. The central peripapillary retinal NFL was 99.82 ± 6.43 μm, and the mean GCL thickness of the fovea was 14.18 ± 1.92 μm. The mean IPL thickness and the mean INL thickness of the fovea were 20.73 ± 1.64 and 17.59 ± 2.89 μm, respectively. The mean OPL and ONL thicknesses were 23.00 ± 2.89 and 88.23 ± 13.21 μm, respectively. The mean RPE thickness was 41.05 ± 16.57 μm. There were no differences in thickness between the two eyes (Supplementary Table S1).

In the 1- to 3-mm zone (parafovea), the TRL thicknesses seemed to differ between the four quadrants as evaluated with the analysis of variance test ($P = 0.022$), and the nasal TRL thickness was thicker than the temporal TRL thickness after Bonferroni correction ($P = 0.020$). Among the four quadrants of parafoveal NFL thickness, the superior thickness was significantly thicker than the temporal and nasal thickness ($P = 0.005$ and $P < 0.001$, respectively), and the inferior thickness was thicker than the nasal and temporal thickness ($P < 0.001$ and $P < 0.001$, respectively). The nasal NFL thickness in the 1- to 3-mm zone was thicker than the temporal NFL thickness ($P = 0.001$). In the 1- to 3-mm zone, the ONL thicknesses seemed to have significant differences ($P = 0.033$); however, there was no difference after Bonferroni correction (Supplementary Table S2 and Fig. 1). All quadrants showed significant differences for the perifoveal (3–6 mm) TRL, IRL, GCC, and NFL thicknesses. The nasal TRL, IRL, GCC, and NFL were the thickest, followed by the inferior, superior, and temporal thicknesses (Supplementary Table S2 and Fig. 1). The IPL was thickest in the nasal quadrant and thinnest in the superior quadrant. Although the INL was thicker in the nasal and inferior regions, its thickness sequentially increased in the temporal and superior regions. There were no significant differences between the inferior and temporal thicknesses for the INL ($P = 0.9999$).

The mean peripheral TRL, GCC, IRL, and ORL thicknesses were 223.55 ± 20.88, 64.00 ± 12.07, 151.84
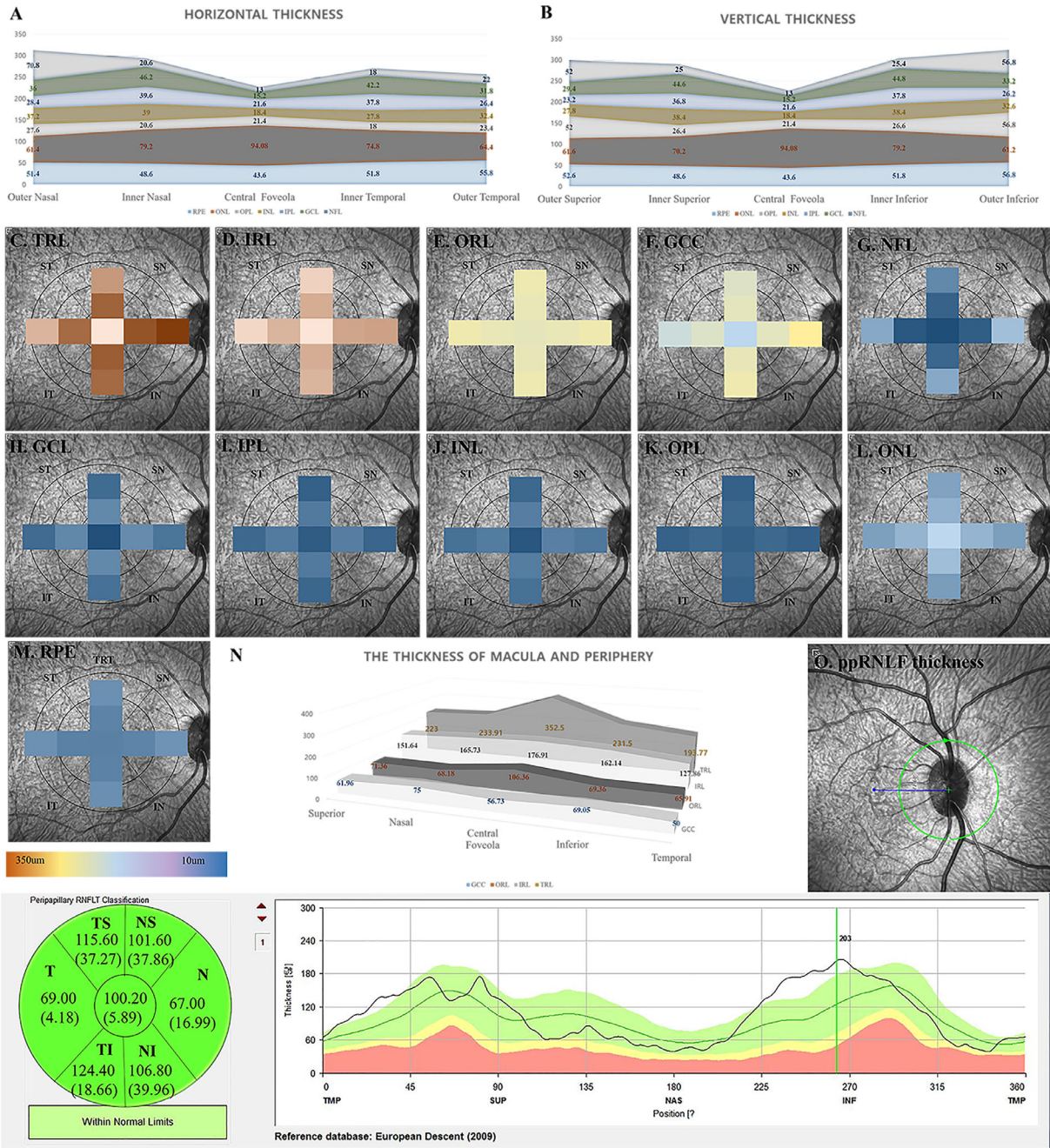
Figure 1. Heat maps and comparison of each retinal sublayer's thickness and the mean thickness of peripapillary retinal nerve fiber layers. (**A**) The comparison of each retinal sublayer's horizontal thickness is shown. Nasal TRL, NFL thickness in the inner ring is thicker than temporal thicknesses. Nasal TRL, IRL, GCC, and NFL thickness in the outer ring are thicker than temporal thicknesses. (**B**) The comparison of each retinal sublayer's vertical thickness is shown. Inferior TRL, IRL, GCC, and NFL thicknesses in the outer ring are thicker than superior thicknesses. (C–M) The heat maps of each sublayer in the ETDRS circle are shown. (**C**) The TRL thickness is shown. In the 1- to 3-mm zone, the nasal TRL is thicker than the temporal TRL. In the 3- to 6-mm zone, the thickness is different among the four quadrants, thickest at nasal, followed by inferior, superior, and temporal. (**D**) The IRL thickness is shown. In the 3- to 6-mm zone, the thickness differs among the four quadrants, thickest at nasal, inferior, superior, and temporal (no significant difference between superior and temporal). (**E**) The ORL thickness is shown. There is no difference between the ORL thickness among the four quadrants in the 1- to 3- and 3- to 6-mm zones. (**F**) The GCC thickness. In the 3- to 6-mm zone, the GCC thickness differs among the four quadrants, thickest at nasal, followed by inferior, superior, and temporal. (**G**) The nerve fiber layer (NFL) thickness is shown. In the 3- to 6-mm zone, the NFL thickness is different among the four quadrants, thickest at nasal, followed by inferior, temporal, and superior (no significant difference between at inferior and at nasal). (**H**) The GCL thickness is shown. No difference among the four quadrants is observed. (**I**) The IPL thickness is shown. In the 3- to 6-mm zone, the superior IPL thickness is thinner than other IPL thicknesses. (**J**) The INL thickness is shown. In the 3- to 6-mm zone, the INL thickness is different among the four quadrants, thickest at nasal, followed by inferior, temporal, and superior (no significant difference between at inferior and at nasal). (**K**) The OPL thickness is shown.

→

←
No difference among the four quadrants is observed. (**L**) The ONL thickness is shown. No difference among the four quadrants is observed. (**M**) The RPE thickness is shown. No difference among the four quadrants is observed. (**N**) The peripheral thickness of GCC, ORL, IRL, and TRL are thinner than those of the foveola. (**O**) The peripapillary retinal NFL (ppRNFL) thickness is shown. Superior and temporal ppRNFL thickness is thicker than nasal and temporal ppRNFL thickness.
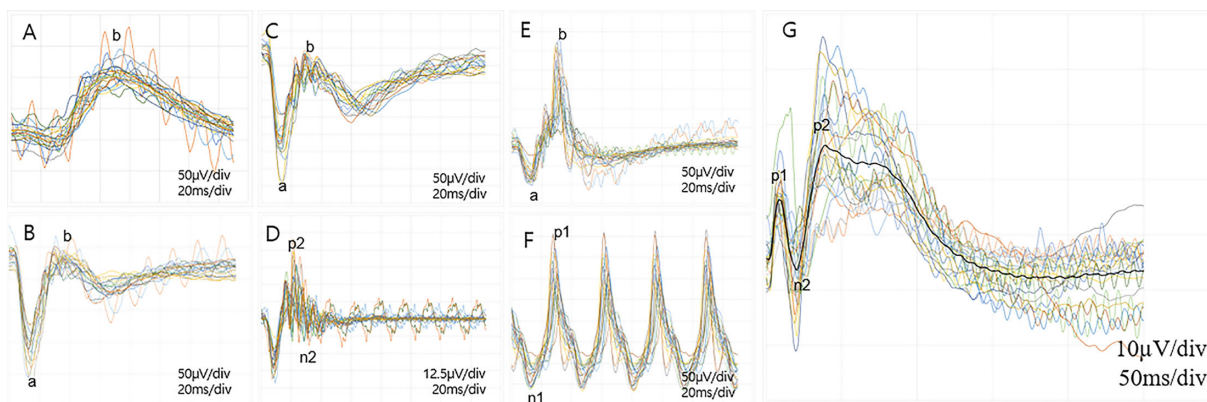

Figure 2. Trace map of the full-field retinography and flash VEPs in all cynomolgus monkeys. (**A**) A scotopic 0.01 ERG showing the mean peak latency and amplitudes of b-wave (71.99 ± 5.23 ms and 96.36 ± 24.46 μV, respectively). (**B**) A scotopic 3.0 ERG showing the mean peak latency of the a-wave and b-wave (14.78 ± 1.00 and 32.89 ± 1.81 ms, respectively). The amplitudes of the a-wave and b-wave are 128.36 ± 31.68 and 132.71 ± 26.34 μV, respectively. (**C**) A scotopic 10.0 ERG showing the mean peak latency of the a-wave and b-wave (13.98 ± 0.94 and 13.98 ± 0.94 ms, respectively). The mean amplitudes of the a-wave and b-wave are 90.97 ± 25.09 and 79.70 ± 19.08 μV, respectively. (**D**) The oscillatory potential with a mean amplitude of 32.34 ± 11.62 μV. (**E**) A photopic 3.0 ERG showing the mean peak latency of the a-wave and b-wave (12.91 ± 1.03 and 31.79 ± 2.16 ms, respectively). The mean amplitudes of the a-wave and b-wave are 27.13 ± 7.39 and 79.86 ± 19.21 μV, respectively. (**F**) The 30-Hz flicker ERG with a mean amplitude of 99.63 ± 26.21 μV. (**G**) The trace map of flash VEP is shown. The p1-wave, the n2-wave, and p-2 wave peak latencies were 18.59 ± 3.24, 39.71 ± 6.71, and 79.76 ± 8.41 ms, respectively.

$\pm$ 18.45, and 68.71 ± 7.54 μm, respectively. The temporal quadrant thicknesses of the TRL, GCC, and IRL were thinner than those of the other quadrants ($P < 0.001$). In the peripheral GCC and IRL thickness, the nasal thickness was also greater than the superior thickness ($P < 0.001$) (Supplementary Table S2).

Electroretinography

The morphology of scotopic and photopic ERG in cynomolgus monkeys was similar to that in humans (Supplementary Fig. S3). The peak latency of the b-wave in the scotopic 0.01 ERG was 71.99 ± 5.23 ms. The peak latency of the a-wave and b-wave in the scotopic and photopic 3.0 ERG was 14.78 ± 1.00 and 32.89 ± 1.81 ms and 12.91 ± 1.03 and 31.79 ± 2.16 ms, respectively. The mean amplitude of the photopic 3.0 flicker ERG was 99.63 ± 26.21 μV. The peak latency and amplitudes of all waves are summarized in Table 1, and all the waves are depicted in Figure 2. There was no difference in the wave peak latency and amplitude between the right and left eyes (Supplementary Table S3). The peak latency of the a-wave in scotopic 3.0 ERG ($r = 0.610$, $P = 0.002$) and the peak latency of the a-wave in the photopic 3.0 ERG ($r = 0.466$, $P = 0.029$) were signif-

icantly correlated with age (Supplementary Fig. S3). In two subgroups (adolescent monkeys <5 years of age and young adults >7 years of age),[23,24] the young adult group showed delayed peak latency of a-wave ($P = 0.021$ by Mann–Whitney U test) in scotopic 3.0 ERG. It delayed the peak latency of the a-wave ($P = 0.027$) and b-wave ($P = 0.049$) in the photopic 3.0 ERG group than in the adolescent group (Supplementary Table S4 and Supplementary Fig. S4).

VEPs

The flash VEP pattern of cynomolgus was not identical to that of human VEP. A small-amplitude p1-wave was followed by a small-amplitude n2-wave and a large-amplitude p2-wave (Fig. 2G). The peak latencies of the p1-wave, n2-wave, and p-2 wave were 18.59 ± 3.24, 39.71 ± 6.71, and 79.76 ± 8.41 ms, respectively. The peak latencies and amplitudes of all the waves are summarized in Table 4. The mean peak latency ($r = -0.444$, $P = 0.039$) and amplitude ($r = -0.551$, $P = 0.008$) of the n-2 wave, the amplitude ($r = -0.708$, $P < 0.001$) of the p2-wave, and the amplitude ($r = -0.518$, $P = 0.013$) of the n-4 wave were significantly correlated with age (Supplementary Fig. S3). In two subgroups (adolescent group vs. young adult

Table 4. Flash VEPs of Cynomolgus Monkeys

	Flash VEP
Mean implicit time of the n1 wave (ms)	3.91 ± 2.20
Mean amplitude of the n1 wave (μV)	1.59 ± 1.14
Mean implicit time of the p1 wave (ms)	18.59 ± 3.24
Mean amplitude of the p1 wave (μV)	11.88 ± 4.33
Mean implicit time of the n2 wave (ms)	39.71 ± 6.71
Mean amplitude of the n2 wave (μV)	15.21 ± 8.07
Mean implicit time of the p2 wave (ms)	79.76 ± 8.41
Mean amplitude of the p2 wave (μV)	27.06 ± 12.67
Mean implicit time of the n3 wave (ms)	116.54 ± 19.56
Mean amplitude of the n3 wave (μV)	7.81 ± 5.47
Mean implicit time of the p3 wave (ms)	143.11 ± 21.21
Mean amplitude of the p3 wave (μV)	5.36 ± 4.61
Mean implicit time of the n4 wave (ms)	330.63 ± 43.69
Mean amplitude of the n4 wave (μV)	24.39 ± 10.48
Mean implicit time of the p4 wave (ms)	403.41 ± 57.40
Mean amplitude of the p4 wave (μV)	4.78 ± 3.68

group),[23,24] the young adult group showed a faster peak latency of the n2-wave ($P = 0.033$ by Mann–Whitney U test), the smaller amplitude of the n2 wave ($P = 0.027$), a smaller amplitude of p2 wave ($P < 0.001$), and smaller amplitude of n4 wave ($P = 0.021$) than the adolescent group (Supplementary Table S4 and Supplementary Fig. S4).

Discussion

We simultaneously presented normative data on visual function, anatomy, and ocular size in cynomolgus monkeys. Monkeys have many anatomical similarities with humans.[25,26] A study comparing the growth of the eyes of monkeys and humans reported that

1 year in a monkey's life is almost equivalent to 3 human years.[27] In our study, the average monkey age was 63.79 ± 20.36 months (median, 52.77 months; range, 49.4–98.83 months), which was the period after sexual maturation. Based on previous studies, this age spectrum is at a stable plateau stage with respect to eye growth.[28] Although cynomolgus monkeys generally have smaller body size and weight (2.5–3.5 kg),[29] their AL (18.41 ± 0.52 mm) is relatively large when compared with the whole body and slightly smaller than the human eye size (16–24 mm depending on age).[30] The eyeball sizes of rhesus monkeys are 18 to 22 mm, which is marginally smaller than that of humans and comparable with or relatively larger than that of cynomolgus monkeys.[28,31] In nonhuman primates, the eyeball volume showed a linear increase to the body weight even in different species.[31] However, we could not obtain a significant correlation between body weight and AL ($P = 0.216$).

The LT of the human and nonhuman primates reportedly increases marginally after birth and decreases at a certain age.[27,31,32] A few studies have shown a further marginal increase at 4 to 15 years.[28,33] In higher age groups, the average LT of a human, rhesus monkey, and cynomolgus monkey is similar at 4.0 to 4.5, 3.5 (range, 2.8–4.0), and 4.0 mm, respectively (Supplementary Table S5).[28,31,34] Although the ACD varies depending on measurement methods, the mean values of average ACD in a human, rhesus monkey, cynomolgus monkey are similar (3.0, 3.5, and 3.2 mm respectively) (Supplementary Table S5).[28,30,31,34] With aging, the thicknesses of the retina, choroid, and sclera decrease[35] and VCD increases.[36] Although the correlation between the AL and the VCD of rhesus monkeys is the highest,[28] our study showed that the AL had significant correlations with both the ACD and the VCD. However, there was no correlation between age and ocular biometry in the study monkeys.

Nonhuman primates have a fovea that is absent in other large animals, such as dogs and pigs. Hence, they are important for preclinical research on macular diseases. The association between OCT and histology was reported in nonhuman primates,[37,38] and the retinal thickness of the macula was significantly thicker than that of the peripheral retina like humans. Our study showed that the TRL, IRL, and ORL thicknesses of the fovea were thicker than those of the peripheral retina. The TRL, IRL, GCC, and ORL thicknesses on the perifovea and parafovea were also thicker than those on the periphery ($P < 0.001$). Parafoveal thicknesses seem to be thicker than those of fovea centers in humans and nonhuman primates.[15,39,40] The thickness trend on the macula was also observed in our study,

except for the GCC. The TRL, IRL, GCL, IPL, INL, OPL, and ONL in the 1- to 3-mm zone (parafovea) was thicker than those in the 1-mm circular zone (fovea), whereas the ORL, NFL, and RPE layers in the 3- to 6-mm zone (perifovea) was thicker than those in the 1-mm circular zone (fovea).

Using cynomolgus monkeys (aged 30–50 months) of Mauritanian genetic background, Denk et al.[40] reported a thicker macular retinal thickness, especially for the parafovea, than that in our study using the same OCT instrument. Except for the foveal thickness (18%), the difference in thickness of each layer was within 10% between the two studies. In humans, the variability in the thickness of the retina depends on race.[41] The nasal retinal thickness of parafoveal quadrants is thicker than the temporal thickness in humans and nonhuman primates and among the different thickness patterns for different parafoveal quadrants, the nasal seems to be thicker.[42] This finding suggests that the NFL bundle has the greatest impact on the different thickness patterns.

In our study, the GCC and IRL thicknesses in the parafoveal and perifoveal quadrants showed significant differences. The thicknesses of the two layers of the nasal quadrants were thicker than those of the temporal quadrants in the 1- to 3-mm zone. In the 3- to 6-mm zones, the NFL, IRL, and GCC were thicker in the order of nasal, inferior, superior, and temporal quadrants, respectively. With respect to the periphery, the TRL, GCC, and IRL were the thickest in the nasal periphery, followed by the inferior, superior, and temporal regions. However, there were no significant differences between the nasal and inferior peripheries in TRL, GCC, and IRL thicknesses.

The VEP is an effective and objective method for evaluating the state of visual pathways. However, the VEP results from nonhuman primates show variable patterns with different peak latencies and amplitudes. The waveform and amplitudes of VEP recordings in primates differed according to the depth of electrodes (deep or superficial from the brain) or recording locations in the striate laminae.[43,44] Using the electrode on the midfrontal lobe, the normal rhesus macaque showed a reversed appearance from our VEP.[45] Our study showed faster peak latencies of p1-, n2-, and p2- waves than other monkeys (Supplementary Table S5).[46] Compared with the previous study using 2- to 3-year-olds, our monkey was older. In our study, age showed a negative correlation with the peak latency of the n2-wave. Age might influence peak latency in addition to race differences (*Macaca fascicularis* vs. *Macaca arcloides*). Therefore, normative data of the VEP from each study setting are needed to observe the change after experiments, such as the induction of

retinal degeneration or the implantation of a retinal prosthesis.

Furthermore, several studies involving nonhuman primate models of retinal diseases have shown functional changes through ERG.[17,47,48] Age and AL are known to be related to b-wave amplitudes, particularly in scotopic ERG.[49,50] Our study also showed a significant correlation between age and the peak latency of the a-wave in the scotopic 3.0 and photopic 3.0 ERG. These results are consistent with those of a previous study on humans (Supplementary Table S5).[49] The ERG of cynomolgus monkeys in the present work showed comparable results to those of other monkeys.[17,18,47,48] Bouskila et al.[18] showed similar peak latency of the a-wave and delayed peak latency of b-wave (36.7 ms) in rod–cone response using green monkeys (Supplementary Table S5). The ERG of cynomolgus monkeys in our study also showed ERG morphology similar to humans. Although the peak latency was similar to that in humans (around 15 ms for a-wave, 32 ms for b-wave), the amplitudes were lower (250–370 μV for b-wave in adults).[51,52] Nonhuman primates have a density of 3.1 million cone cells and 61.0 million rod cells; the distribution being similar to that in humans.[53] The similarity of photoreceptor density with smaller eyeball sizes may have generated similar peak latency and relatively lower amplitudes in cynomolgus monkey's ERG compared with those in humans.[17,54]

We have been cautious in interpreting the correlations between each parameter because of the relatively few animals. First, the VCD was negatively correlated with the LT, and the AL was positively correlated with ACD and VCD (Supplementary Fig. S2). Previous studies with nonhuman primates including, cynomolgus monkeys, also showed a decreased proportion of ACD and VCD related to the increased proportion of LT with eye growth.[27,31]

Our study has some limitations. All examinations were performed under general anesthesia. It is thus possible that the ERG amplitude and peak latency may have been affected. In dogs, general anesthesia significantly decreases amplitudes than sedation, especially in dark-adaptive ERG.[55] However, a previous study has shown that sevoflurane (which was used in this study) has little effect on ERG amplitudes, and its use significantly attenuates the VEP amplitudes.[56] Second, our study included relatively few monkeys. All cynomolgus monkeys were young adults after sexual maturation and had full eye growth; all were male. Further studies using a larger sample size with a wider age range and both sexes will help understand the normative values of cynomolgus monkeys' eyes.

Nevertheless, our study could provide normative data of monkeys among the same cynomolgus species, which varies to some extent by species and region. We simultaneously presented ocular biometry, electrophysiology, and OCT thickness findings, including those for the fovea and periphery of cynomolgus monkeys, which are good candidates for preclinical studies of ocular diseases. Therefore, our normative data will be useful as baseline data to evaluate subtle changes in visual function and retinal anatomy, especially in the cynomolgus monkey retinal degeneration model.

Acknowledgments

Contributors: Study design (K.E.C., S.W.K.); conduct of the study (K.E.C., V.T.Q.A., S.W.K.); data collection (K.E.C., Y.J.K., H.C.J., H.J.E., D.K.S.); analysis and interpretation of the data (K.E.C., C.M.Y., S.W.K.); and preparation, review, and approval of the manuscript (all authors).

Disclosure: **K.-E. Choi,** None; **V.T.Q. Anh,** None; **C. Yun,** None; **Y.-J. Kim,** None; **H. Jung,** None; **H. Eom,** None; **D. Shin,** None; **S.-W. Kim,** None

References

1. Chang B. Mouse models for studies of retinal degeneration and diseases. *Methods Mol Biol*. 2013;935:27–39.
2. Koh AE, Alsaeedi HA, Rashid MBA, et al. Retinal degeneration rat model: a study on the structural and functional changes in the retina following injection of sodium iodate. *J Photochem Photobiol B*. 2019;196:111514.
3. Jeon CJ, Strettoi E, Masland RH. The major cell populations of the mouse retina. *J Neurosci Res*. 1998;18:8936–8946.
4. Lozano DC, Twa MD. Development of a rat schematic eye from in vivo biometry and the correction of lateral magnification in SD-OCT imaging. *Invest Ophthalmol Vis Sci*. 2013;54:6446–6455.
5. Freeberg FE, Nixon GA, Reer PJ, et al. Human and rabbit eye responses to chemical insult. *Fundam Appl Toxicol*. 1986;7:626–634.
6. Regal S, O'Connor D, Brige P, Delattre R, Djenizian T, Ramuz M. Determination of optical parameters of the porcine eye and development of a simulated model. *J Biophotonics*. 2019;12:e201800398.
7. Chandler MJ, Smith PJ, Samuelson DA, MacKay EO. Photoreceptor density of the domestic pig retina. *Vet Ophthalmol*. 1999;2:179–184.
8. Yamaue Y, Hosaka YZ, Uehara M. Spatial relationships among the cellular tapetum, visual streak and rod density in dogs. *J Vet Med Sci*. 2015;77:175–179.
9. Picaud S, Dalkara D, Marazova K, Goureau O, Roska B, Sahel JA. The primate model for understanding and restoring vision. *Proc Natl Acad Sci USA*. 2019;116:26280–26287.
10. Ikeda Y, Nishiguchi KM, Miya F, et al. Discovery of a cynomolgus monkey family with retinitis pigmentosa. *Invest Ophthalmol Vis Sci*. 2018;59:826–830.
11. Kennedy C, Des Rosiers MH, Sakurada O, et al. Metabolic mapping of the primary visual system of the monkey by means of the autoradiographic [14C]deoxyglucose technique. *Proc Natl Acad Sci USA*. 1976;73:4230–4234.
12. Nauhaus I, Nielsen KJ, Disney AA, Callaway EM. Orthogonal micro-organization of orientation and spatial frequency in primate primary visual cortex. *Nat Neurosci*. 2012;15:1683–1690.
13. Roosing S, Thiadens AA, Hoyng CB, Klaver CC, den Hollander AI, Cremers FP. Causes and consequences of inherited cone disorders. *Prog Retin Eye Res*. 2014;42:1–26.
14. Yan G, Zhang G, Fang X, et al. Genome sequencing and comparison of two nonhuman primate animal models, the cynomolgus and Chinese rhesus macaques. *Nat Biotechnol*. 2011;29:1019–1023.
15. Denk N, Maloca PM, Steiner G, et al. Retinal features in cynomolgus macaques (Macaca fascicularis) assessed by using scanning laser ophthalmoscopy and spectral domain optical coherence tomography. *Comparative Med*. 2020;70:145–151.
16. Anger EM, Unterhuber A, Hermann B, et al. Ultrahigh resolution optical coherence tomography of the monkey fovea. Identification of retinal sublayers by correlation with semithin histology sections. *Exp Eye Res*. 2004;78:1117–1125.
17. Bee WH. Standardized electroretinography in primates: a non-invasive preclinical tool for predicting ocular side effects in humans. *Curr Opin Drug Discov Devel*. 2001;4:81–91.

18. Bouskila J, Javadi P, Palmour RM, Bouchard JF, Ptito M. Standardized full-field electroretinography in the Green Monkey (Chlorocebus sabaeus). *PLoS One*. 2014;9:e111569.

19. Lin KH, Tran T, Kim S, et al. Advanced retinal imaging and ocular parameters of the rhesus macaque eye. *Transl Vis Sci Techn*. 2021;10:7.

20. Giannakaki-Zimmermann H, Munk MR, Ebneter A, Wolf S, Zinkernagel M. Automated retinal layer segmentation and their thickness profiles in healthy subjects: a comparison of 55 degrees wide-field and conventional 30 degrees spectral domain-optical coherence tomography. *Retina J Ret Vit Dis*. 2020;40:2004–2009.

21. McCulloch DL, Marmor MF, Brigell MG, et al. ISCEV Standard for full-field clinical electroretinography (2015 update). *Doc Ophthalmol*. 2015;130:1–12.

22. Odom JV, Bach M, Brigell M, et al. ISCEV standard for clinical visual evoked potentials: (2016 update). *Doc Ophthalmol*. 2016;133:1–9.

23. Kiely P, Crewther S, Nathan J, Brennan N, Efron N, Madigan M. A comparison of ocular development of the Cynomolgus monkey and man. *Clin Vis Sci*. 1987;1:269–280.

24. Choi K, Chang J, Lee MJ, et al. Reference values of hematology, biochemistry, and blood type in cynomolgus monkeys from Cambodia origin. *Lab Anim Res*. 2016;32:46–55.

25. Hendrickson A, Zhang C. Development of cone photoreceptors and their synapses in the human and monkey fovea. *J Comp Neurol*. 2019;527:38–51.

26. Dawson WW, Ulshafer RJ, Engel HM, Hope GM, Kessler MJ. Macular disease in related rhesus-monkeys. *Doc Ophthalmol*. 1989;71:253–263.

27. Kiely PM, Crewther SG, Nathan J, Brennan NA, Efron N, Madigan M. A comparison of ocular development of the cynomolgus monkey and man. *Clin Vision Sci*. 1987;1:269–280.

28. Fernandes A, Bradley DV, Tigges M, Tigges J, Herndon JG. Ocular measurements throughout the adult life span of rhesus monkeys. *Invest Ophthalmol Vis Sci*. 2003;44:2373–2380.

29. Rosso MC, Badino P, Ferrero G, Costa R, Cordero F, Steidler S. Biologic data of cynomolgus monkeys maintained under laboratory conditions. *PLoS One*. 2016;11:e0157003.

30. Bhardwaj V, Rajeshbhai GP. Axial length, anterior chamber depth-a study in different age groups and refractive errors. *J Clin Diagn Res*. 2013;7:2211–2212.

31. Augusteyn RC, Maceo Heilman B, Ho A, Parel JM. Nonhuman primate ocular biometry. *Invest Ophthalmol Vis Sci*. 2016;57:105–114.

32. Augusteyn RC. On the growth and internal structure of the human lens. *Exp Eye Res*. 2010;90:643–654.

33. Wendt M, Croft MA, McDonald J, Kaufman PL, Glasser A. Lens diameter and thickness as a function of age and pharmacologically stimulated accommodation in rhesus monkeys. *Exp Eye Res*. 2008;86:746–752.

34. Qiao-Grider Y, Hung LF, Kee CS, Ramamirtham R, Smith EL, 3rd. Normal ocular development in young rhesus monkeys (Macaca mulatta). *Vision Res*. 2007;47:1424–1444.

35. Augusteyn RC, Nankivil D, Mohamed A, Maceo B, Pierre F, Parel JM. Human ocular biometry. *Exp Eye Res*. 2012;102:70–75.

36. Larsen JS. The sagittal growth of the eye. IV. Ultrasonic measurement of the axial length of the eye from birth to puberty. *Acta Ophthalmol (Copenh)*. 1971;49:873–886.

37. Yiu G, Wang Z, Munevar C, et al. Comparison of chorioretinal layers in rhesus macaques using spectral-domain optical coherence tomography and high-resolution histological sections. *Exp Eye Res*. 2018;168:69–76.

38. Anger EM, Unterhuber A, Hermann B, et al. Ultrahigh resolution optical coherence tomography of the monkey fovea. Identification of retinal sublayers by correlation with semithin histology sections. *Exp Eye Res*. 2004;78:1117–1125.

39. Nieves-Moreno M, Martinez-de-la-Casa JM, Cifuentes-Canorea P, et al. Normative database for separate inner retinal layers thickness using spectral domain optical coherence tomography in Caucasian population. *PLoS One*. 2017;12:e0180450.

40. Denk N, Maloca P, Steiner G, et al. Macular thickness measurements of healthy, naive cynomolgus monkeys assessed with spectral-domain optical coherence tomography (SD-OCT). *PLoS One*. 2019;14:e0222850.

41. Asefzadeh B, Cavallerano AA, Fisch BM. Racial differences in macular thickness in healthy eyes. *Optom Vis Sci*. 2007;84:941–945.

42. Patel PJ, Foster PJ, Grossi CM, et al. Spectral-domain optical coherence tomography imaging in 67 321 adults: associations with macular thickness in the UK Biobank Study. *Ophthalmology*. 2016;123:829–840.

43. Schroeder CE, Tenke CE, Givre SJ, Arezzo JC, Vaughan HG, Jr. Striate cortical contribution to

the surface-recorded pattern-reversal VEP in the alert monkey. *Vision Res*. 1991;31:1143–1157.

44. Givre SJ, Schroeder CE, Arezzo JC. Contribution of extrastriate area V4 to the surface-recorded flash VEP in the awake macaque. *Vision Res*. 1994;34:415–428.

45. Fortune B, Wang L, Bui BV, Burgoyne CF, Cioffi GA. Idiopathic bilateral optic atrophy in the rhesus macaque. *Invest Ophthalmol Vis Sci*. 2005;46:3943–3956.

46. Creel DJ, Dustman RE, Beck EC. Visually evoked responses in the rat, guinea pig, cat, monkey, and man. *Exp Neurol*. 1973;40:351–366.

47. Bouskila J, Harrar V, Javadi P, et al. Scotopic vision in the monkey is modulated by the G protein-coupled receptor 55. *Vis Neurosci*. 2016;33:E006.

48. Liu C-N, Peng Q, Yates DW, Huang W, Devantier H, Aguirre SA. Ocular safety assessment of sodium iodate in cynomolgus monkeys: characterization of a classic retinal toxicant. *Toxicol Res*. 2017;1:2397847317696370.

49. Weleber RG. The effect of age on human cone and rod ganzfeld electroretinograms. *Invest Ophthalmol Vis Sci*. 1981;20:392–399.

50. Westall CA, Dhaliwal HS, Panton CM, et al. Values of electroretinogram responses according to axial length. *Doc Ophthalmol*. 2001;102:115–130.

51. Rangaswamy NV, Frishman LJ, Dorotheo EU, Schiffman JS, Bahrani HM, Tang RA. Photopic ERGs in patients with optic neuropathies: comparison with primate ERGs after pharmacologic blockade of inner retina. *Invest Ophthalmol Vis Sci*. 2004;45:3827–3837.

52. Birch DG, Anderson JL. Standardized full-field electroretinography. Normal values and their variation with age. *Archives of ophthalmology (Chicago, Ill: 1960)*. 1992;110:1571–1576.

53. Wikler KC, Rakic P. Distribution of photoreceptor subtypes in the retina of diurnal and nocturnal primates. *J Neurosci Res*. 1990;10:3390–3401.

54. Wikler KC, Williams RW, Rakic P. Photoreceptor mosaic: number and distribution of rods and cones in the rhesus monkey retina. *J Comp Neurol*. 1990;297:499–508.

55. Lin SL, Shiu WC, Liu PC, Cheng FP, Lin YC, Wang WS. The effects of different anesthetic agents on short electroretinography protocol in dogs. *J Vet Med Sci*. 2009;71:763–768.

56. Tanaka R, Tanaka S, Ichino T, Ishida T, Fuseya S, Kawamata M. Differential effects of sevoflurane and propofol on an electroretinogram and visual evoked potentials. *J Anesth*. 2020;34:298–302.